HHS Public Access

Author manuscript

Cell Calcium. Author manuscript; available in PMC 2016 December 01.

Published in final edited form as:

Cell Calcium. 2015 December ; 58(6): 589–597. doi:10.1016/j.ceca.2015.09.006.

Crosstalk Between Purinergic Receptors and Canonical Signaling Pathways in the Mouse Salivary Gland

Sumit Bhattacharya, **John F. Imbery**, **Prince Tuffour Ampem**, and **David R. Giovannucci***

Department of Neurosciences, University of Toledo Medical Center, Toledo, OH, USA

1. Introduction

Saliva production is positively regulated by cholinergic and adrenergic autonomic neural input and crosstalk between these signaling pathways to facilitate secretory activity has been demonstrated extensively [1-5]. In addition to these canonical pathways, a non-cholinergic non-adrenergic (NANC) pathway regulating protein and fluid secretion [6-9] has also been implicated. One of the primary candidates for NANC input is via activation of ionotropic purinergic receptors [10-16]. Moreover, we recently demonstrated that ionotropic P2X4 and P2X7 receptor (P2X4R and P2X7R) activation can contribute to Ca^{2+} dynamics and protein exocytosis in acinar cells isolated from the mouse parotid salivary gland [17].

In the current study we investigated whether there was crosstalk between the canonical Ca^{2+} signaling pathways and the NANC/purinergic signaling pathway. Enhancement of P2X4R- or P2X7R-mediated intracellular calcium ($[Ca^{2+}]_i$) rises was revealed following ß-adrenergic receptor (β-AR) activation. Although this signaling was largely mediated by receptor activation and a PKA-dependent mechanism, direct activation of PKA or Epac using pharmacological compounds could also enhance P2X-mediated Ca^{2+} signals. Additionally, we assessed whether there was crosstalk between muscarinic receptor mediated and P2X receptor mediated signaling. In these experiments a selective P2X7R blocker was used [18, 19] to investigate whether exocytotic activity evoked by muscarinic receptor activation induced luminal ATP release and P2X7R activation. The current study furthers our understanding of how canonical Ca^{2+} pathways in conjunction with NANC Ca^{2+} signaling pathways may integrate to regulate $[Ca^{2+}]_i$ levels and secretory activity in the parotid gland.

*Corresponding author at: University of Toledo Medical Center, Department of Neurosciences, 3000 Arlington avenue, Toledo, OH 43614, USA, Tel: +1 419 383 5004; Fax: +1 419 383 3008. david.giovannucci@utoledo.edu (Corresponding author David R. Giovannucci).

Author Contributions S.B. designed experiments, acquired and analyzed data and wrote the manuscript, P.A. and J.I acquired and analyzed data and D.G. conceived and directed the research, reviewed the data, wrote and edited the manuscript.

Declaration of Interest There is no conflict of interest.

2. Materials and methods

2.1 Animal use

Male NIH Swiss Webster mice (18–25 g; Charles River Laboratories International, Inc., Wilmington, MA, USA) were euthanized by CO_2 asphyxiation and puncture of the heart. All experiments using animals were approved by and carried out in strict accordance with the policies of the University of Toledo Institutional Animal Care and Use Committee and conformed to the Guide for the Care and Use of Laboratory Animals, National Institutes of Health Publication No. 85-23 (National Research Council, National Academy Press, Washington, DC, 1996).

2.2 Chemicals

Adenosine 5′-triphosphate disodium salt hydrate (ATP), 2′(3′)-O-(4-Benzoylbenzoyl)adenosine 5′-triphosphate triethylammonium salt (Bz-ATP), 3-Isobutyl-1-methylxanthine (IBMX), carbamoylcholine chloride (CCh), isoproterenol hydrochloride (ISO) and forskolin (FRSK) were obtained from Sigma Chemicals (St Louis, MO, USA). 2-Aminoethoxydiphenylborate (2-APB) was purchased from Calbiochem (San Diego, CA, USA). 8-(4-Chlorophenylthio) adenosine 3', 5'-cyclic monophosphate (8-CPT) and cAMP-dependent protein kinase inhibitor peptide (myristoylated-14-22) amide (PKI) were obtained from Enzo Life Sciences (Farmingdale, NY, USA). 1-(2, 3-Dichlorophenyl)-*N*-[[2-(2-pyridinyloxy) phenyl]methyl]-1*H*-tetrazol-5-amine (A839977), a potent P2X7R antagonist and 8-pCPT-2-O-Me-cAMP-AM were obtained from Tocris Bioscience (Bristol, UK).

2.3 Isolation of parotid acini

Dispersed mouse parotid acini were obtained by collagenase digestion [20]. Dissected parotid glands were minced with scissors. The minced glands were subjected to step-wise digestion by suspension in 20 ml of Eagle's minimal essential medium containing collagenase-P (0.04 mg/ml; Roche Applied Science, Indianapolis, IN, USA), 0.01% glutamine and 1% bovine serum albumin (BSA). Parotid gland pieces were subjected to 20 min incubation. This step was followed by two 15 min incubations in collagenase digestion solution with shaking (65 rpm) at 37°C. After the first incubation, centrifugation was performed at 210 × *g* for 1 min. The pellet was resuspended in a fresh aliquot of oxygenated solution. Next, parotid tissue pieces were passed through glass fire-polished pipettes with progressively smaller tips. Following digestion, dispersed parotid acini were rinsed in basal Eagle's medium (BME) without BSA and centrifuged at 70 × *g* for 1 min. The pellet was resuspended in 20 ml of attachment BME solution containing 0.01% glutamine, 0.02% penicillin–streptomycin (Sigma Aldrich, St. Louis, MO, USA) and 1% BSA. Parotid acinar clumps were loaded with 5 μM fura-2AM (Calbiochem, San Diego, CA, USA) for 30–40 min for live cell imaging.

2.4 Live cell fluorescence and time differentiated imaging

Live cell imaging was performed using a Polychrome IV monochromator-based high-speed digital imaging system (TILL Photonics, Gräfelfing, Germany) ported to a fiber optic guide and epifluorescence condenser and coupled to a Nikon TE2000 microscope equipped with

DIC optics. Cytosolic Ca^{2+} concentration dynamics in fura-2 AM-loaded acinar cells was recorded by alternatively illuminating the acinar clumps with dual wavelength light (340 and 380 nm) focused onto the image plane via a DM400 dichroic mirror and Nikon Super- Fluor ×40 oil-immersion objective, and fluorescence obtained through a 525nm ± 25 nm band-pass filter (Chroma Technologies, Brattleboro, VT, USA) [17]. Alternating transmitted light and fluorescent images were acquired using a high-speed Uniblitz VS35 optical shutter (Vincent Associates, Rochester, NY, USA) placed in the tungsten lamp illumination path. Exocytotic activity was measured from transmitted light images using time-differentiated imaging, a validated method for optically quantifying acinar cell zymogen granule fusion [20, 21]. Pairs of transmitted light and fluorescence images (30 and 50 ms exposure, respectively) were collected at 1-2Hz. Images were generated by subtracting each transmitted light frame from its preceding frame as described previously [20]. Acquired images were analyzed using TillVisION (TILL Photonics) and ImageJ (W. S. Rasband, National Institutes of Health, Bethesda, MD, USA). For estimating changes in free cytosolic Ca^{2+} concentration, an in vitro calibration was achieved using the 340 nm/380 nm signal ratio and buffers containing known $[Ca^{2+}]$ concentrations. The change in $[Ca^{2+}]_i$ was calculated using the equation $[Ca^{2+}]_i = [(R - R_{min})/R_{max} - R] *(S_f/S_b)*K_d$, where R was the experimental ratio value of the 340 nm to 380 nm signal, R_{max} was the ratio value in the presence of saturating Ca^{2+}, R_{min} was the ratio value in Ca^{2+} free buffer, S_f/S_b was the ratio of 380 nm fluorescence under Ca^{2+} free and saturating conditions, and K_d for fura-2 was taken from literature value. The values of R_{max}, R_{min}, S_f/S_b and K_d were 13.7, 0.57, 20 and 225 nM, respectively. Calibration and imaging was performed at room temperature and fluorescence background was subtracted prior to calculation of ratio values. Because of variability in the kinetics of the responses, the evoked amplitude change in $[Ca^{2+}]_i$ was quantified as the difference between the pre-stimulus baseline value and the maximal amplitude of the response measured in the first 60 s following application of agonist.

For statistical analysis, GraphPad Prism 3 (GraphPad Software Inc., La Jolla, CA, USA) software packages were used and values represented as the mean ± standard error. Statistical significance was determined using Student's *t* test and *p* values of less than 0.05 were considered statistically significant.

3. Results

Saliva production is regulated by autonomic neural inputs that generate the intracellular second messengers inositol 1,4,5 trisphosphate ($InsP_3$) and cyclic adenosine monophosphate (cAMP) to promote fluid secretion and protein exocytosis [22, 23]. Although muscarinic receptor activation results in Ca^{2+}-evoked fluid and protein secretion, the majority of sustained protein secretion is induced by adrenergic receptor activation. Previous studies demonstrated that simultaneous activation of muscarinic receptors and ß-AR signaling pathways leads to synergistic enhancement of the evoked increase in $[Ca^{2+}]_i$ in salivary gland acinar cells [24-27]. This is largely mediated by cAMP induced PKA phosphorylation of $InsP_3Rs$ [1, 4]. However, whether ß-AR activation amplifies Ca^{2+} signals induced by purinoceptor activation has not been thoroughly investigated. Because both ATP and norepinephrine are co-packaged into large dense core vesicles (LDCV) at adrenergic nerve terminals [28-30] it is likely that these neurotransmitters are released together during

sympathetic nerve stimulation to potentially activate both signaling pathways. A precedent for crosstalk between muscarinic receptors and purinergic receptors has been demonstrated in mouse lacrimal glands [31], yet this line of inquiry remains less studied in the parotid gland.

3.1 Crosstalk between β-AR and P2X4R leads to potentiation of ATP-evoked $[Ca^{2+}]_i$ signals in parotid acinar cells

In these sets of experiments, we evoked Ca^{2+} signals in mouse parotid acinar cells by application of 10 μM ATP, a concentration we have previously shown to preferentially activate P2X4Rs [17]. The evoked signals were compared between groups that were treated with vehicle or with chemical modulators of cAMP signaling. A marked enhancement in free $[Ca^{2+}]_i$ was observed following pharmacological elevation of cAMP levels compared to control groups. As shown in Fig 1A and 1B, following treatment with 8-cpt-cAMP (a synthetic cAMP analogue), forskolin (FRSK, the adenyl cyclase activator) or IBMX (a phosphodiesterase inhibitor), the ATP-evoked maximal free $[Ca^{2+}]_i$ signals were enhanced around 2- to 4-fold compared to control acini exposed to ATP alone.

To determine whether the enhancement of P2X4R-evoked Ca^{2+} signals in the presence of cAMP modulators was mediated by PKA, we tested whether the FRSK induced enhancement of the Ca^{2+} signal was modulated following incubation with the PKA-selective inhibitor PKI. As shown in Fig 2A and B, following pre-treatment with PKI the FRSK-induced enhancement of the Ca^{2+} signals was largely abolished. This finding is consistent with a previously reported PKA dependent mechanism that alters the expression of P2X4R protein at the plasma membrane [32].

Because pharmacological manipulations to increase cAMP levels do not necessarily recapitulate the spatial or temporal characteristics of cAMP dynamics induced by endogenous receptor activation, we determined the peak ATP-evoked Ca^{2+} signal amplitudes prior to or following treatment with the β-adrenergic agonist isoprenaline (ISO). ISO treatment alone produced negligible increases in resting $[Ca^{2+}]_i$ during 10 min of application (change in resting $[Ca^{2+}]_i$ levels was less than 2.3 nM ± 0.8 nM, n = 3). However, as shown in Fig 3A and B, ISO treatment significantly enhanced the ATP evoked $[Ca^{2+}]_i$ change where the average ATP-evoked changes in free $[Ca^{2+}]_i$ levels with or without ISO treatment was 26.3 nM ± 1.2 nM and 13.7 nM ± 2.1 nM, respectively. Additionally, this enhancement was largely suppressed by PKI treatment. The maximal amplitude of the evoked Ca^{2+} change following ISO treatment in the presence of PKI was 15.4 nM ± 4.3 nM. These data suggested that the enhancement of the evoked $[Ca^{2+}]_i$ response during β-AR activation was largely mediated through a PKA-dependent mechanism, although a contribution from another cAMP-binding protein such as Epac could not be excluded (see 3.3 below).

3.2 Crosstalk between β-AR and P2X7R potentiates Bz-ATP-evoked $[Ca^{2+}]_i$ signals in parotid acinar cells

In a previous study we showed that, in contrast to P2X4R mediated Ca^{2+} signals, a major component of the P2X7R-evoked change in $[Ca^{2+}]_i$ was mediated by Ca^{2+} induced Ca^{2+}

release (CICR) from the endoplasmic reticulum [17]. Because CICR is thought to be enhanced following PKA mediated phosphorylation of the type I $InsP_3$ receptor [3, 4], we investigated whether an enhancement of CICR resulted in an indirect crosstalk between β-ARs and P2X7Rs (Fig 4).

Similar to our approach to P2X4R, we tested the effect of pharmacological elevation of cAMP on the $[Ca^{2+}]_i$ signals evoked by the P2X7R-selective agonist Bz-ATP. Fig 4A shows a set of representative $[Ca^{2+}]_i$ responses from acinar cells treated with Bz-ATP alone or in the presence of either 8-CPT-cAMP or FRSK. Treatment with either of these compounds potentiated the evoked Ca^{2+} transient by nearly 3-fold compared to the control responses (Fig 4B).

We also tested whether this enhancement was dependent on PKA. As shown in Fig 5A, a significant enhancement of the evoked $[Ca^{2+}]_i$ changes was induced by co-stimulation of P2X7R and ß-AR. Indeed, ISO and Bz-ATP treated cells showed more than a 2-fold increase in the evoked Ca^{2+} transient (Fig 5B). This enhancement was largely abrogated by treatment with the IP_3R blocker 2-APB and probably mediated in part by PKA phosphorylation of the IP_3 receptor and enhanced CICR. To determine this, we tested whether PKA activation contributed to the enhancement of the evoke change in $[Ca^{2+}]_i$ using PKI to block PKA activity (Fig 5A and 5C). As shown, in Fig 5A and 5C, PKI treatment largely abolished the potentiation of $[Ca^{2+}]_i$ change. This suggested that PKA-mediated phosphorylation of IP_3Rs and augmentation of CICR may largely underlie the enhancement of the $[Ca^{2+}]_i$ response during co-activation of P2X7R and ß-AR.

3.3 Epac activation enhanced P2X4R- and P2X7R-evoked changes in Ca^{2+}

Although cAMP is a ubiquitous second messenger and widely known as an activator of protein kinase A, it can also activate the cAMP-binding guanine nucleotide exchange factor, Epac. Our results using the inhibitor PKI suggested that the enhancements in the P2X4R and P2X7R evoked Ca^{2+} responses are largely mediated through PKA. However, Epac activation has recently been shown to accelerate Ca^{2+} waves in pancreatic acini [33]. Thus, we tested whether Epac activation might also enhance the Ca^{2+} changes evoked by P2X receptor activation. Because currently available Epac inhibitors are either general protein denaturants or only selective for Epac 2 that is expressed preferentially in the brain, we addressed this question using the cell-permeable selective Epac activator, cAMP analog 8-pCPT-2-O-Me-cAMP-AM (8-pCPT-2-O-Me). In this set of experiments we monitored P2X4R- or P2X7R-evoked Ca^{2+} changes in acini that were pre-treated with vehicle control or Epac activator. As shown in Figure 6A and B, acini treated with 1.5 μM 8-pCPT-2-O-Me showed a significant enhancement in both the P2X4 and P2X7 mediated Ca^{2+} changes. Treatment with 2-APB abolished this effect and, given that previous work has demonstrated Epac-mediated modulation of ryanodine receptors, suggested the involvement of CICR. However, the mechanism and relevance of these observations is not immediately clear.

3.4 Luminal P2X7R activation contributes to Ca^{2+} signals evoked by muscarinic receptor activation

Muscarinic receptor type 3 (M3R) activation has been shown to evoke Ca^{2+}-dependent zymogen granule exocytosis in acinar cells of the salivary gland and exocrine pancreas [28, 34-39]. The exocytotic events typically occurred at the apical (subluminal) and lateral aspects of the acinar cells when monitored by multi-photon and time-differentiated imaging methods [17, 20, 21]. Recently, we demonstrated that P2X7Rs are enriched in the subluminal region of acinar cells and exhibit overlap with the sites of Ca^{2+} signal initiation and exocytosis [17]. In addition, Irena Novak's group showed that zymogen granules of the exocrine pancreas contained ATP that was released during exocytotic activity [40]. Thus we tested the hypothesis that P2X7Rs in parotid acinar cells are activated by ATP-released from zymogen granules during exocytotic activity, and that this activation can contribute to the CCh-evoked Ca^{2+} signal. To assess whether P2X7Rs were activated during CCh treatment, we evoked and monitored exocytosis at different rates (number of exocytotic events/cell/min) by treating acinar cells with a range of concentrations of CCh. We then monitored the Ca^{2+} dynamics before or following the selective inhibition of the P2X7R by treatment with the P2X7 selective, structurally novel antagonist, A839977. Prior to this assessment, we investigated whether treatment with the P2X7R antagonist had any off-target effect on M3R-evoked Ca^{2+} signals or exocytotic activity. This was achieved using HEK 293 cells stably expressing muscarinic type 3 receptors or following CCh-evoked exocytotic activity by time differentiated imaging analysis.

As shown in Fig 7A, treatment with A839977 did not diminish $[Ca^{2+}]_i$ changes evoked by 2 μM CCh. The average changes in peak amplitude with or without antagonist treatment was 742 nM ± 55 nM and 634 nM ± 105 nM, respectively. Likewise, A839977 treatment did not appear to alter exocytotic rates. As shown in Fig 7B, application of 0.1 μM, 2 μM or 10 μM CCh induced a concentration-dependent increase in exocytotic activity that was not significantly altered by A839977 treatment. Thus, we used A839977 to test whether CCh-evoked exocytotic activity induced luminal P2X7R activation and contributed to M3R-evoked Ca^{2+} signals in acinar cells. A839977 treatment had no effect on Ca^{2+} signals evoked by 0.1 μM CCh, an agonist concentration that only weakly activated exocytotic activity (Fig 7C). In contrast, A839977 was found to significantly diminish the Ca^{2+} signal amplitude evoked by 2 μM and 10 μM CCh, agonist concentrations that activated robust exocytotic activity (Fig 7D and 7E). Figure 7F shows the averaged maximal amplitudes for the evoked responses with or without inclusion of A839977. These data are consistent with the notion that luminal ATP accumulation during sustained exocytosis may activate apical P2X7Rs and contribute to CCh-evoked Ca^{2+} signals.

4. Discussion

Over the last half-century, deconvolution of the biochemical pathways in living cells has elucidated the individual molecular circuits that selectively drive specific life processes and revealed that multiple individual circuits can interact and influence one another. For example in living tissues, cells can receive distinct extracellular inputs that induce the simultaneous activation, interaction and integration of signal transduction pathways. These

interactions are referred to as signal crosstalk and might profoundly affect phenotypic output. The work presented here substantiates an effort to peel apart an integrated signaling circuit that regulates the production of primary saliva.

Typically, sympathetic and parasympathetic drive works in opposition to manifest a “gas-and-brake” relationship to maintain physiological homeostasis. One notable exception to this paradigm occurs in the salivary glands where both pathways of autonomic control positively induce the secretion of primary saliva at the acinar cell level [41-44]. Moreover, it is likely that the activation of these pathways is largely co-incident and works in relative concert to tune secretory output according to physiologic need. Indeed, there is ample evidence that adrenergic and cholinergic signaling act in a synergistic manner to promote protein and salt secretion [3, 4]. What is less understood is the degree to which the so-called non-adrenergic, non-cholinergic (NANC) pathway that is also recruited during autonomic drive contributes to salivation or the extent to which this pathway is subject to crosstalk with the canonical pathways to modulate Ca^{2+} signals and secretory output.

A number of studies by our group and others suggested that there is crosstalk between purinergic and canonical signaling pathways. For example, findings from Brown et al suggested that PKA-mediated phosphoregulation plays an indirect role in modulating P2X4R channel function or assembly [32]. Studies conducted on DT-40 chicken B cells and HEK293 cells points towards PKA dependent receptor trafficking and inhibition of P2X4R endocytosis leading to increase in P2X4R expression on the plasma membrane [45]. Although indirect phosphoregulation by PKA is thought to be the dominant signal by which P2XR function is modified, the current study also points to a possible role for Epac as a potential modulator of P2XR signaling under specific conditions. This effect was perhaps due to sensitization of CICR as treatment with 2-APB resulted in abolishment of this enhancement. Although the mechanism by which Epac might enhance CICR and the physiological relevance of these observations is not clear, a better understanding of these questions would benefit from siRNA approaches or the development of effective Epac inhibitors that are beyond the scope of the current study.

In addition, we showed that activation of P2X7 receptors that are enriched at the luminal border evoked robust Ca^{2+} signals that were dominated by Ca^{2+} induced Ca^{2+} release contributions [17]. Given the apical distributions of P2X7Rs [46], intracellular Ca^{2+} release channels and the sites of zymogen granule fusion, we hypothesized that muscarinic receptor activation, via exocytotic activity at the apical membrane, would increase ATP levels in the lumen. Subsequent activation of P2X7 receptors would thus lead to luminal Ca^{2+} influx and Ca^{2+} signal amplification via CICR. Indeed, Novak’s group had previously suggested this possibility and showed that zymogen granules in mice contained ATP [47]. Advancing this idea, we showed that selective blockage of P2X7Rs reduced the muscarinic receptor activation evoked Ca^{2+} responses only during stimulations that induced exocytotic activity, suggesting that localized Ca^{2+} entry through P2X7Rs can facilitate CICR and support a feed forward mechanism to enhance $InsP_3$ mediated Ca^{2+} signals.

Our finding is consistent with a study conducted on lacrimal glands where cholinergic and P2X7R agonists induced increases in $[Ca^{2+}]_i$ that was larger than that evoked by a single

agonist but that was less than additive [31] suggesting that these pathways used the same internal Ca^{2+} store. In contrast, other studies have shown an apparent antagonistic relationship between muscarinic and purinergic signaling. For example one study demonstrated enhanced muscarinic receptor-evoked $[Ca^{2+}]_i$ rises in parotid acini isolated from P2X7R knockout mice compared to the background strain [48], and another study on submandibular gland acini showed that ATP and CCh co-stimulation decreased fluid secretion in wild type mice [16]. The differences in findings between groups are not immediately clear but may be related to differences in the agonist concentrations, mouse strains or tissues used.

Because the major, canonical signal transduction pathways can act synergistically to control the rate, volume and composition of primary saliva, acinar cells provide a test bed for studying the integration of molecular signaling to achieve a defined physiological output. An important observation of the current study is that crosstalk between signaling pathways might not be exclusive to the canonical pathways. Our study points to a critical association between canonical and non-canonical pathways to modulate the rate and magnitude of secretory activity. This adds another potential layer of complexity to establish greater control of fluid secretion and protein exocytosis and to expand the dynamic range of physiological output. For example, protein secretion in the parotid occurs during both stimulated and unstimulated phases [49]. How signal crosstalk contributes to output during such wide ranges of activity is not well understood but is a focus for further investigation.

Acknowledgments

The authors wish to thank Dr. Andrea Kalinoski in the Advanced Microscopy and Imaging Core at the University of Toledo Health Science Campus for assistance with some of the experiments.

Funding This work was supported by NIDCR grant DE023418.

References

1. Giovannucci DR, Groblewski GE, Sneyd J, Yule DI. Targeted phosphorylation of inositol 1,4,5-trisphosphate receptors selectively inhibits localized Ca2+ release and shapes oscillatory Ca2+ signals. J Biol Chem. 2000; 275:33704–33711. [PubMed: 10887192]
2. Giovannucci DR, Sneyd J, Groblewski GE, Yule DI. Modulation of InsP(3) receptor properties by phosphorylation: Targeting of PKA to InsP(3) receptors shapes oscillatory calcium signals in pancreatic acinar cells. Journal of Korean Medical Science. 2000; 15:S55–S56. [PubMed: 10981516]
3. Straub SV, Giovannucci DR, Bruce JIE, Yule DI. A role for phosphorylation of inositol 1,4,5-trisphosphate receptors in defining calcium signals induced by peptide agonists in pancreatic acinar cells. J Biol Chem. 2002; 277:31949–31956. [PubMed: 12065595]
4. Bruce JIE, Shuttleworth TJ, Giovannucci DR, Yule DI. Phosphorylation of inositol 1,4,5-trisphosphate receptors in parotid acinar cells - A mechanism for the synergistic effects of cAMP on Ca2+ signaling. J Biol Chem. 2002; 277:1340–1348. [PubMed: 11694504]
5. Ahuja M, Jha A, Maleth J, Park S, Muallem S. cAMP and Ca2+ signaling in secretory epithelia: Crosstalk and synergism. Cell Calcium. 2014; 55:385–393. [PubMed: 24613710]
6. Ekstrom J. Role of nonadrenergic, noncholinergic autonomic transmitters in salivary glandular activities in vivo, Frontiers of Oral Biology; Neural mechanisms of salivary gland secretion. 1999:94–130.
7. Tobin G, Ekstrom J. Parasympathetic Nanc-Secretion of Saliva in the Mink, and Effects of Substance-P and Vip, Regul. Pept. 1992; 39:95–101.

8. Ekstrom J, Ekstrom PF. Depletion of acinar secretory granules in the ferret parotid gland: Effects of substance P and vasoactive intestinal peptide. Exp Physiol. 1998; 83:727–735. [PubMed: 9782183]
9. Gallacher DV. SUBSTANCE-P IS A FUNCTIONAL NEUROTRANSMITTER IN THE RAT PAROTID-GLAND. Journal of Physiology-London. 1983; 342:483–498.
10. Turner JT, Weisman GA, Landon LA, Park M, Camden JM. Salivary gland nucleotide receptors: Evidence for functional expression of both P2X and P2Y subtypes. Eur J Morphol. 1998; 36:170–175. [PubMed: 9825916]
11. Soltoff SP, Mcmillian MK, Cragoe EJ, Cantley LC, Talamo BR. Effects of Extracellular Atp on Ion-Transport Systems and [Ca-2+]I in Rat Parotid Acinar-Cells - Comparison with the Muscarinic Agonist Carbachol. J Gen Physiol. 1990; 95:319–346. [PubMed: 1689766]
12. Soltoff SP, Mcmillian MK, Lechleiter JD, Cantley LC, Talamo BR. Elevation of [Ca-2+]I and the Activation of Ion Channels and Fluxes by Extracellular Atp and Phospholipase C-Linked Agonists in Rat Parotid Acinar-Cells. Ann NY Acad Sci. 1990; 603:76–92. [PubMed: 1705402]
13. Soltoff SP, Mcmillian MK, Talamo BR. Atp Activates a Cation-Permeable Pathway in Rat Parotid Acinar-Cells. Am J Physiol. 1992; 262:C934–C940. [PubMed: 1566819]
14. Erb L, Liao ZJ, Seye CI, Weisman GA. P2 receptors: intracellular signaling, Pflugers Arch. 2006; 452:552–562.
15. Burnstock G, Kennedy C. A Dual Function for Adenosine 5'-Triphosphate in the Regulation of Vascular Tone - Excitatory Cotransmitter with Noradrenaline from Perivascular Nerves and Locally Released Inhibitory Intravascular Agent. Circ Res. 1986; 58:319–330. [PubMed: 3013455]
16. Nakamoto T, Brown DA, Catalan MA, Gonzalez-Begne M, Romanenko VG, Melvin JE. Purinergic P2X(7) Receptors Mediate ATP-induced Saliva Secretion by the Mouse Submandibular Gland. J Biol Chem. 2009; 284:4815–4822. [PubMed: 19097994]
17. Bhattacharya S, Verrill DS, Carbone KM, Brown S, Yule DI, Giovannucci DR. Distinct contributions by ionotropic purinoceptor subtypes to ATP-evoked calcium signals in mouse parotid acinar cells. J Physiol-London. 2012; 590:2721–2737. [PubMed: 22451435]
18. Honore P, Donnelly-Roberts D, Namovic M, Zhong CM, Wade C, Chandran P, Zhu C, Carroll W, Perez-Medrano A, Iwakura Y, Jarvis MF. The antihyperalgesic activity of a selective P2X7 receptor antagonist, A-839977, is lost in IL-1 alpha beta knockout mice. Behavioural Brain Research. 2009; 204:77–81. [PubMed: 19464323]
19. Friedle SA, Curet MA, Watters JJ. Recent patents on novel P2X(7) receptor antagonists and their potential for reducing central nervous system inflammation, Recent patents on CNS drug discovery. 2010; 5:35–45.
20. Chen Y, Warner JD, Yule DI, Giovannucci DR. Spatiotemporal analysis of exocytosis in mouse parotid acinar cells. American Journal of Physiology-Cell Physiology. 2005; 289:C1209–C1219. [PubMed: 16000640]
21. Warner JD, Peters CG, Saunders R, Won JH, Betzenhauser MJ, Gunning WT, Yule DI, Giovannucci DR. Visualizing form and function in organotypic slices of the adult mouse parotid gland. Am J Physiol-Gastr L. 2008; 295:G629–G640.
22. Gibbins HL, Carpenter GH. Alternative Mechanisms of Astringency - What Is the Role of Saliva? Journal of Texture Studies. 2013; 44:364–375.
23. Carpenter GH, Osailan SM, Correia P, Paterson KP, Proctor GB. Rat salivary gland ligation causes reversible secretory hypofunction. Acta Physiologica. 2007; 189:241–249. [PubMed: 17305704]
24. Tanimura A, Nezu A, Tojyo Y, Matsumoto Y. Isoproterenol potentiates alpha-adrenergic and muscarinic receptor-mediated Ca2+ response in rat parotid cells. American Journal of Physiology-Cell Physiology. 1999; 276:C1282–C1287.
25. Hirono C, Sugita M, Furuya K, Yamagishi S, Shiba Y. Potentiation by isoproterenol on carbachol-induced K+ and Cl- currents and fluid secretion in rat parotid. Journal of Membrane Biology. 1998; 164:197–203. [PubMed: 9662563]
26. Watson EL, Jacobson KL, Dijulio DH, Dowd FJ. Biphasic Effects of Carbachol on Stimulated Camp Accumulation in Mouse Parotid Acini. Am J Physiol. 1993; 265:C1061–C1068. [PubMed: 7694473]

27. Watson EL, Wu ZL, Jacobson KL, Storm DR, Singh JC, Ott SM. Capacitative Ca2+ entry is involved in cAMP synthesis in mouse parotid acini. American Journal of Physiology-Cell Physiology. 1998; 274:C557–C565.
28. Sorensen CE, Novak I. Visualization of ATP release in pancreatic acini in response to cholinergic stimulus - Use of fluorescent probes and confocal microscopy. J Biol Chem. 2001; 276:32925–32932. [PubMed: 11387334]
29. Novak I. ATP as a signaling molecule: The exocrine focus. News in Physiological Sciences. 2003; 18:12–17. [PubMed: 12531926]
30. Harkins AB, Fox AP. Activation of purinergic receptors by ATP inhibits secretion in bovine adrenal chromaffin cells. Brain Research. 2000; 885:231–239. [PubMed: 11102577]
31. Dartt DA, Hodges RR. Cholinergic Agonists Activate P2X(7) Receptors to Stimulate Protein Secretion by the Rat Lacrimal Gland. Investigative Ophthalmology & Visual Science. 2011; 52:3381–3390. [PubMed: 21421880]
32. Brown DA, Bruce JIE, Straub SV, Yule DI. CAMP potentiates ATP-evoked calcium signaling in human parotid acinar cells. J Biol Chem. 2004; 279:39485–39494. [PubMed: 15262999]
33. Shah AU, Grant WM, Latif SU, Mannan ZM, Park AJ, Husain SZ. Cyclic AMP accelerates calcium waves in pancreatic acinar cells. Am J Physiol-Gastr L. 2008; 294:G1328–G1334.
34. Ohnishi H, Ernst SA, Wys N, McNiven M, Williams JA. Rab3D localizes to zymogen granules in rat pancreatic acini and other exocrine glands. Am J Physiol. 1996; 271:G531–538. [PubMed: 8843780]
35. Ishikawa Y, Cho G, Yuan Z, Skowronski MT, Pan Y, Ishida H. Water channels and zymogen granules in salivary glands. J Pharmacol Sci. 2006; 100:495–512. [PubMed: 16799262]
36. Riedel D, Antonin W, Fernandez-Chacon R, Alvarez de Toledo G, Jo T, Geppert M, Valentijn JA, Valentijn K, Jamieson JD, Sudhof TC, Jahn R. Rab3D is not required for exocrine exocytosis but for maintenance of normally sized secretory granules. Molecular and cellular biology. 2002; 22:6487–6497. [PubMed: 12192047]
37. Kogel T, Rudolf R, Hodneland E, Copier J, Regazzi R, Tooze SA, Gerdes HH. Rab3D Is Critical for Secretory Granule Maturation in PC12 Cells. Plos One. 2013; 8
38. Field RB, Kruse DH, Redman RS. Immunohistochemical localization and mRNA detection of Rab3D and/or Rab3B in rat von Ebner's glands, parotid gland, pancreas, and liver. The Histochemical journal. 2001; 33:71–77. [PubMed: 11432642]
39. Messenger SW, Falkowski MA, Groblewski GE. Ca2+-regulated secretory granule exocytosis in pancreatic and parotid acinar cells. Cell Calcium. 2014; 55:369–375. [PubMed: 24742357]
40. Haanes KA, Novak I. ATP storage and uptake by isolated pancreatic zymogen granules. Biochem J. 2010; 429:303–311. [PubMed: 20441565]
41. Proctor GB, Carpenter GH. Regulation of salivary gland function by autonomic nerves. Autonomic Neuroscience-Basic & Clinical. 2007; 133:3–18. [PubMed: 17157080]
42. Emmelin N. Nerve Interactions in Salivary-Glands. Journal of Dental Research. 1987; 66:509–517. [PubMed: 3305629]
43. Ekstrom J. Autonomic control of salivary secretion, Proceedings of the Finnish Dental Society. Suomen Hammaslaakariseuran toimituksia. 1989; 85:323–331. discussion 361-323. [PubMed: 2699762]
44. Ambudkar IS. Dissection of Calcium Signaling Events in Exocrine Secretion. Neurochem Res. 2011; 36:1212–1221. [PubMed: 21534000]
45. Brown DA, Yule DI. Protein kinase A regulation of P2X(4) receptors: Requirement for a specific motif in the C-terminus. Bba-Mol Cell Res. 2010; 1803:275–287.
46. Chen X, Ernst SA, Williams JA. Dominant negative Rab3D mutants reduce GTP-bound endogenous Rab3D in pancreatic acini. The Journal of biological chemistry. 2003; 278:50053–50060. [PubMed: 14522985]
47. Hede SE, Amstrup J, Christoffersen BC, Novak I. Purinoceptors evoke different electrophysiological responses in pancreatic ducts - P2Y inhibits K+ conductance, and P2X stimulates cation conductance. J Biol Chem. 1999; 274:31784–31791. [PubMed: 10542200]

48. Novak I, Jans IM, Wohlfahrt L. Effect of P2X(7) receptor knockout on exocrine secretion of pancreas, salivary glands and lacrimal glands. J Physiol-London. 2010; 588:3615–3627. [PubMed: 20643770]

49. Gorr SU, Venkatesh SG, Darling DS. Parotid secretory granules: Crossroads of secretory pathways and protein storage. Journal of Dental Research. 2005; 84:500–509. [PubMed: 15914585]

Highlights

- Crosstalk between β-AR and P2X4R potentiates $[Ca^{2+}]_i$ signals in parotid acinar cells
- Crosstalk between β-AR and P2X7R enhances $[Ca^{2+}]_i$ rises in parotid acinar cells
- Exocytotic release of ATP and activation of P2X7R enhances CCh evoked $[Ca^{2+}]_i$ signals

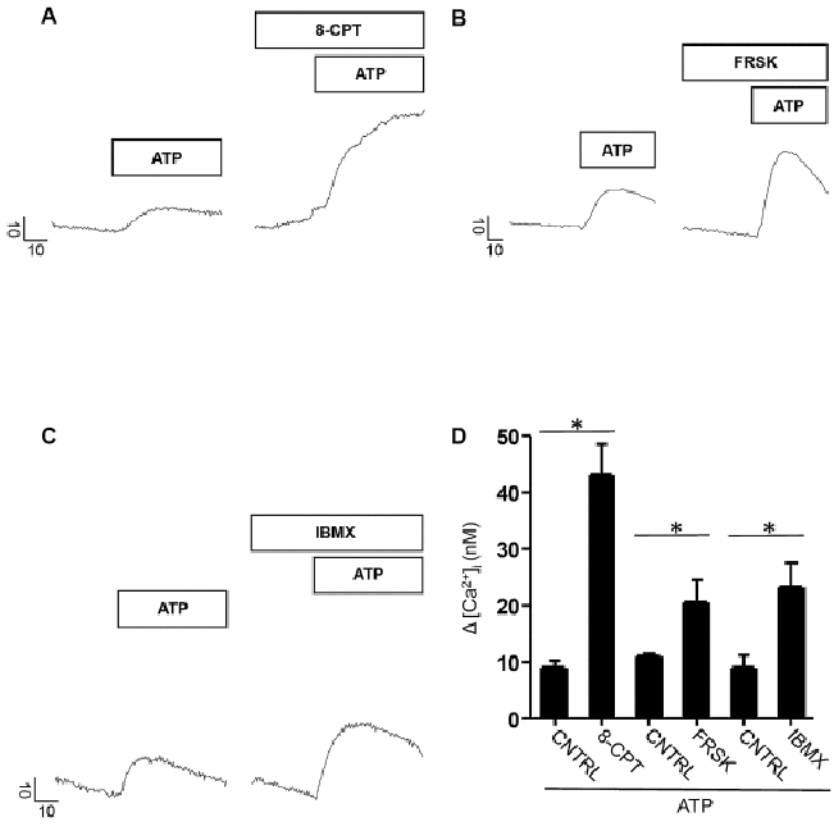

Figure 1.

Pharmacological elevations of cAMP enhanced P2X4R evoked changes in $[Ca^{2+}]_i$ levels. **A - C.** Representative line traces showing maximal Δ $[Ca^{2+}]_i$ evoked by 10 μM ATP alone or following treatment with 1 mM 8-CPT, 10 μM FRSK and 100 μM IBMX respectively. Bars above line traces indicate application of compounds. Vertical scale bar indicates Δ $[Ca^{2+}]_i$ (nM) and horizontal scale bar shows time in seconds (s). Prestimulus $[Ca^{2+}]_i$ values for representative control cell (CNTRL, ATP only) and treated cell traces were 155.3 nM and 293.5 nM (ATP + 8-CPT), 82.7 nM and 118 nM (ATP + FRSK), 188.7 nM and 167.9 nM (ATP + IBMX) respectively. **D.** Bar graph depicts maximal Δ $[Ca^{2+}]_i$ following ATP application in standard recording saline, ($3 \leq n \leq 5$) or co-application with either 8-CPT ($n = 4$) or FRSK ($n = 3$) or IBMX ($n = 5$) respectively. Changes in $[Ca^{2+}]_i$ levels were significantly greater during co-treatment with ATP and 8-CPT ($p < 0.0001$), FRSK ($p < 0.003$) or IBMX ($p < 0.002$). Significant difference from control values as indicated by asterisk (*). Prestimulus $[Ca^{2+}]_i$ values for control and treated bars were 147.4 ± 5.3 nM and 181.4 ± 46 nM (ATP + 8-CPT), 91.8 ± 3.5 nM and 117.9 ± 10.2 nM (ATP + FRSK) and 175.7 ± 6.1 nM and 187.8 ± 13.4 nM (ATP + IBMX) respectively. Parotid acinar cells were pretreated with 8-CPT, FRSK, and IBMX for 10–15 minutes in the above experiments prior to ATP challenge.

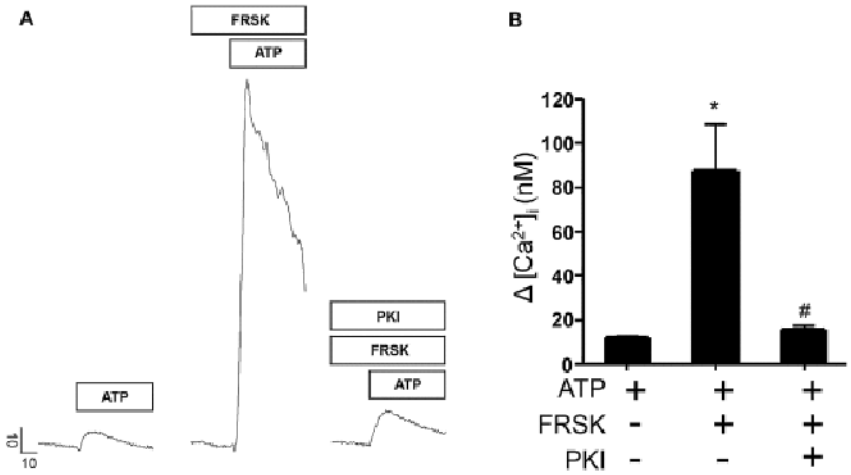

Figure 2.

PKA dependent modulation of P2X4R evoked changes in $[Ca^{2+}]_i$ levels. **A.** Representative line traces depicting Δ $[Ca^{2+}]_i$ evoked by 10 μM ATP with or without treatment with 10 μM FRSK or FRSK and 100 nM PKI respectively. Vertical scale bar indicates Δ $[Ca^{2+}]_i$ (nM) and horizontal scale bar shows time in seconds (s). Prestimulus $[Ca^{2+}]_i$ values for representative control and treated cell traces were 186.6 nM (ATP), 195.5 nM (ATP + FRSK) and 160.1 nM (ATP + FRSK + PKI) respectively. **B.** Bar graph showing maximal Δ $[Ca^{2+}]_i$ following stimulation with ATP alone (n = 9) or co-treated with FRSK (n = 5) or FRSK and PKI (n = 4). Maximal Δ $[Ca^{2+}]_i$ was significantly enhanced in acinar cells following treatment with FRSK ($p < 0.0002$) compared to those stimulated with ATP only. Enhancement of $[Ca^{2+}]_i$ responses was significantly diminished in cells treated with FRSK and PKI ($p < 0.02$). Significant difference from control values or between FRSK groups with or without treatment with PKI indicated by symbols * or # respectively. Treatments are indicated by + and − signs. Prestimulus $[Ca^{2+}]_i$ values for representative control and treated bars were 143.2 ± 4.7 nM (ATP), 227.4 ± 31.7 nM (ATP + FRSK) and 255.3 ± 77.5 nM (ATP + FRSK + PKI) respectively. Acinar cells were pretreated with FRSK or FRSK and PKI for 10-15 minutes before ATP treatment in experiments where these compounds were applied.

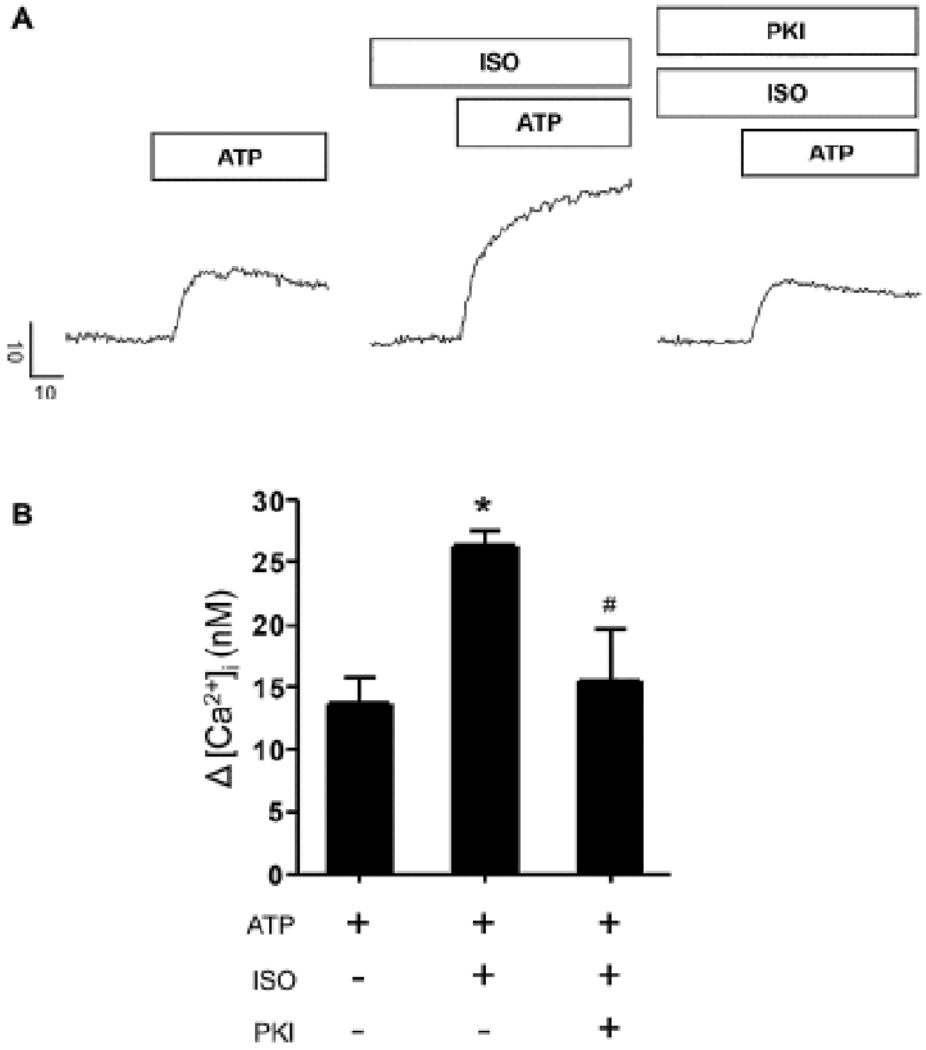

Figure 3.

Co-activation of β-AR and P2X4R resulted in PKA dependent enhancement of $[Ca^{2+}]_i$ changes. **A.** Representative line traces showing maximal Δ $[Ca^{2+}]_i$ responses evoked by 10 μM ATP alone or with 4 μM ISO in the presence or absence of 100 nM PKI. Scale bars indicate Δ $[Ca^{2+}]_i$ in nM and time in seconds (s). Prestimulus $[Ca^{2+}]_i$ values for representative control and treated cell traces were 66.9 nM (ATP), 146.2 nM (ISO) and 111.8 nM (ISO + PKI) respectively. **B.** Bar graph shows maximal change in $[Ca^{2+}]_i$ during ATP treatment alone (*n* = 7) or upon co-treatment with either ISO (*n* = 6) or ISO and PKI (*n* = 4). Treatments are indicated by + and – signs. Significant difference from control or between ISO treated groups is mediated by * and # symbols respectively. Prestimulus $[Ca^{2+}]_i$ values for representative control and treated bars were 144.1 ± 12.2 nM (ATP), 206 ± 9.8 nM (ATP + ISO) and 135.1 ± 7.7 nM (ATP + ISO + PKI) respectively. Acinar cells were pretreated with ISO or ISO and PKI for 15-20 minutes prior to ATP challenge in experiments where these pharmacological compounds were used.

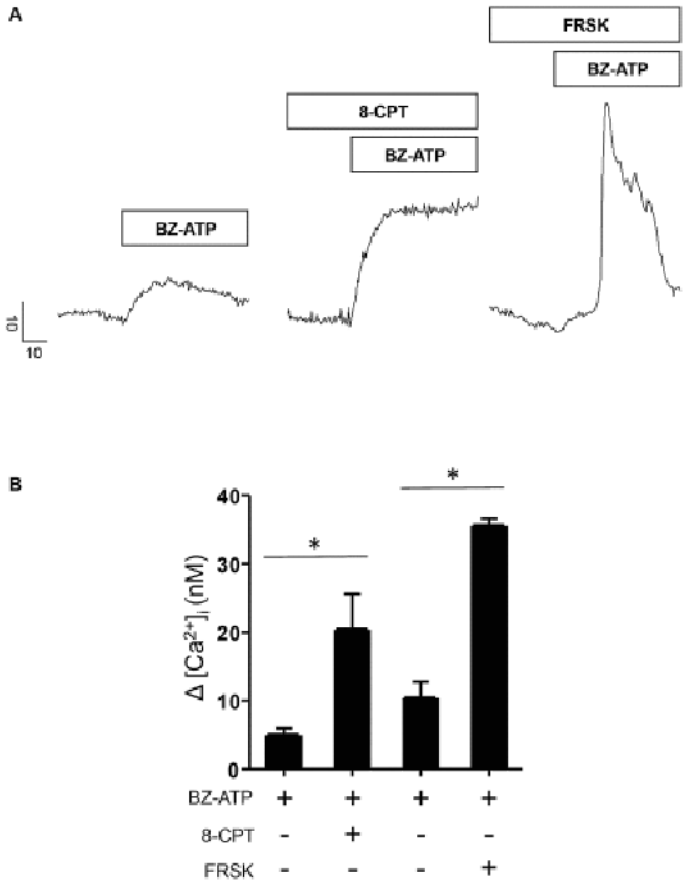

Figure 4.

Elevation of cAMP during P2X7R activation potentiated ATP evoked $[Ca^{2+}]_i$ signals. **A.** Representative line traces depicting maximal Δ $[Ca^{2+}]_i$ evoked by 100 μM BZ-ATP application or upon co-application with either (1 mM) 8-CPT or (10 μM) FRSK. Scale bars indicate Δ $[Ca^{2+}]_i$ (nM) and time in seconds (s). Prestimulus $[Ca^{2+}]_i$ values for representative control and treated cell traces were 162.1 nM (BZ-ATP), 163.7 nM (BZ-ATP + 8-CPT) and 161.8 nM (BZ-ATP + FRSK) respectively. **B.** Bar graph showing maximal Δ $[Ca^{2+}]_i$ upon BZ-ATP application (n = 6) or during 8-CPT (n = 3) or FRSK (n = 3) stimulation. Prestimulus $[Ca^{2+}]_i$ values for representative control and treated bars were 157.7 ± 2.9 nM (BZ-ATP), 156.3 ± 6 nM (BZ-ATP + 8-CPT) and 162.4 ± 7.5 nM (BZ-ATP + FRSK) respectively. Significant difference from control values as indicated by asterisk (*). Acinar cells were pretreated with 8-CPT or FRSK for 10-15 minutes prior to BZ-ATP treatment.

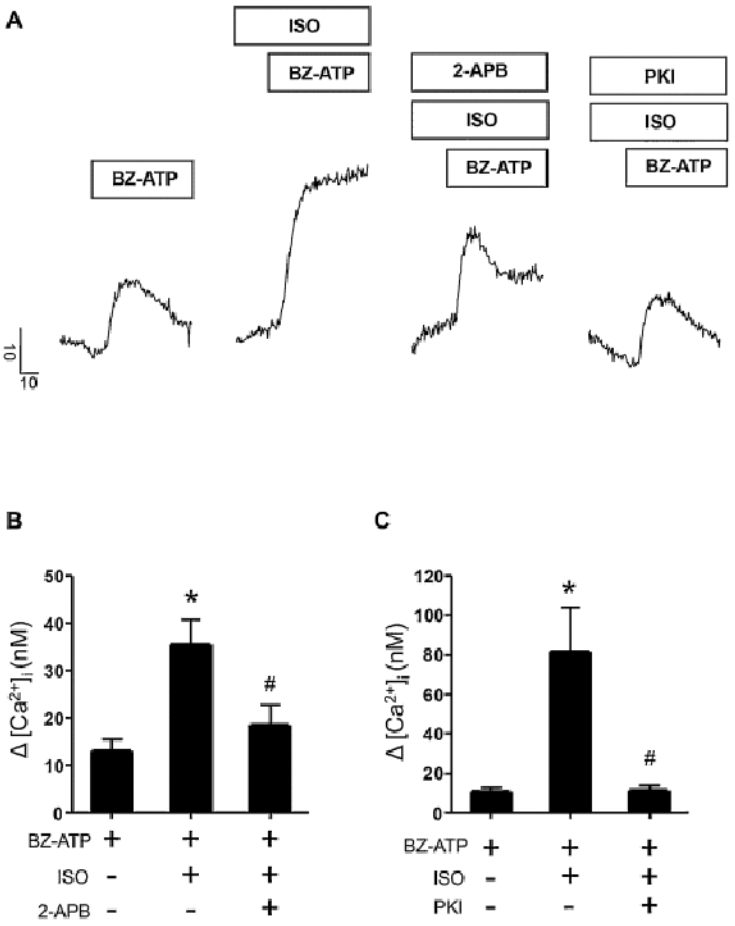

Figure 5.

Co-activation of β-AR and P2X7R induced PKA dependent rises in $[Ca^{2+}]_i$ levels dominated by Ca^{2+} release. **A.** Representative line traces show maximal Δ $[Ca^{2+}]_i$ responses evoked by 100 μM BZ-ATP alone or following 4 μM ISO application or upon ISO and 200 μM 2-APB or ISO and 100 nM PKI treatment. Vertical scale bar indicates Δ $[Ca^{2+}]_i$ (nM) and horizontal scale bar shows time in seconds (s). Prestimulus $[Ca^{2+}]_i$ values for control cell and treated cell traces were 148.3 nM (BZ-ATP), 132.9 nM (BZ-ATP + ISO), 212.1 nM (BZ-ATP + ISO + 2-APB) and 188.7 nM (BZ-ATP + ISO + PKI). **B.** Bar graph showing BZ-ATP evoked changes in $[Ca^{2+}]_i$ upon BZ-ATP application alone (n = 4) or in combination with ISO (n = 3) or ISO and 2-APB (n = 5). The enhancement in $[Ca^{2+}]_i$ levels by ISO treatment was diminished by 2-APB application. Prestimulus $[Ca^{2+}]_i$ values for representative control and treated bars were 151.4 ± 5 nM (BZ-ATP), 111.7 ± 13 nM (BZ-ATP + ISO) and 143.6 ± 12.1 nM (BZ-ATP + ISO + 2-APB) respectively. **C.** Bar graph depicting maximal Δ $[Ca^{2+}]_i$ after exposure to BZ-ATP alone (n = 3) or following ISO (n = 3) or ISO and PKI (n = 3) treatment. Significant differences from control values or between ISO groups with or without treatment with PKI are indicated by symbols (*) and (#) respectively. Prestimulus $[Ca^{2+}]_i$ values for representative control and treated bars were 159.7 ± 3.2 nM (BZ-ATP), 132.7 ± 22.9 nM (BZ-ATP + ISO) and 99.2 ± 6.3 nM (BZ-ATP + ISO + PKI) respectively. Acinar cells were pretreated with ISO or ISO and PKI or ISO

and 2-APB for 15-20 minutes prior to ATP challenge in experiments where these compounds were used.

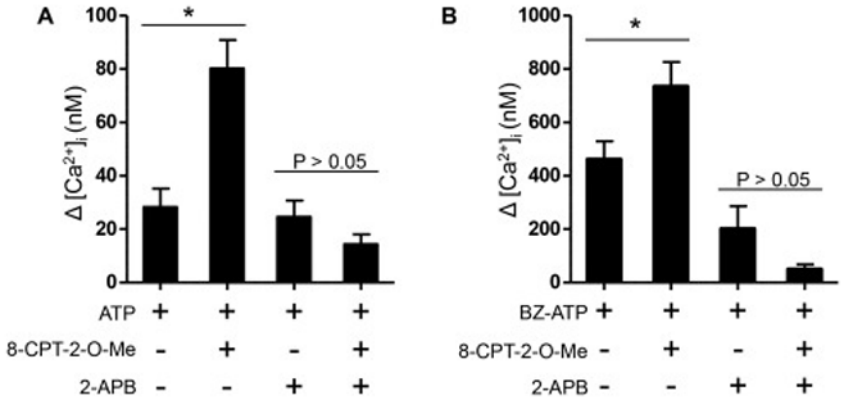

Figure 6.

An Epac-dependent process may contribute to an enhanced Ca^{2+} signal. **A**. Bar graph showing the $\Delta [Ca^{2+}]_i$ following treatment with 1.5 μM 8-pCPT-2-O-Me-cAMP-AM, a selective and cell-permeable activator of EPAC and 10 μM ATP. Controls were 28.3 nM ± 7 nM, n = 4 and 8-pCPT-2-O-Me treated acini were 80.2 nM ± 10.7 nM, p=0.0064, n = 4. Enhancement of the evoked signal was not likely a result of increased Ca^{2+} entry through P2X4 receptors as treatment with 2-APB showed no significant difference when compared to controls (14.4 nM ± 3.7 nM, p=0.1732, n = 5). Prestimulus $[Ca^{2+}]_i$ values for representative control and treated bars were 226.5 ± 8.5 nM (ATP), 242.5 ± 23 nM (ATP + 8-pCPT-2-O-Me), 199.1 ± 23.2 nM (ATP + 2-APB) and 239 ± 14.2 nM (ATP + 8-pCPT-2-O-Me + 2-APB) respectively. **B**. Activation of Epac induced enhancement of the P2X7R-evoked response. 8- pCPT-2-O-Me treated acini displayed a significant enhancement of the BZ-ATP-evoked Ca^{2+} response (734.8 nM ± 91.3 nM, n = 7) compared to control cells (461.1 nM ± 68.7 nM, p=0.04, n = 6). Control acini were not significantly different (24.6 nM ± 6.1 nM, n = 4) from 8-pCPT-2- O-Me treated acini (14.4 nM ± 3.7 nM, p=0.1775, n = 5) in the presence of 2-APB. Prestimulus $[Ca^{2+}]_i$ values for representative control and treated bars were 228.8 ± 4.3 nM (BZ-ATP), 254.6 ± 7.8 nM (BZ-ATP + 8-pCPT-2-O-Me), 206 ± 24.6 nM (BZ-ATP + 2-APB) and 246.2 ± 16.8 nM (BZ-ATP + 8-pCPT-2-O-Me + 2-APB) respectively.

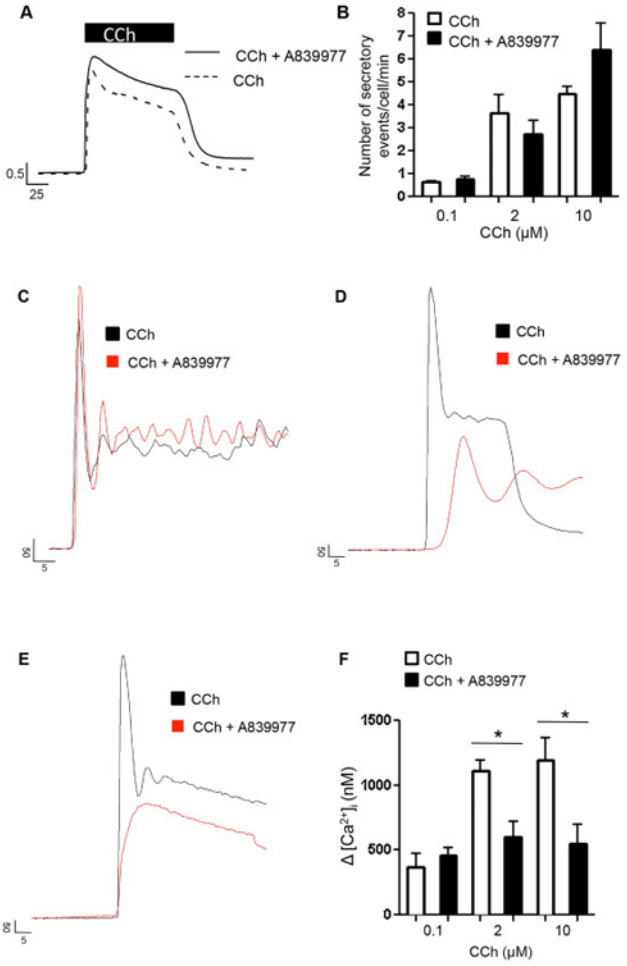

Figure 7.

CCh evoked signaling in the presence or absence of the P2X7R blocker. **A.** Line traces depict maximal Δ $[Ca^{2+}]_i$ (shown in ratio units) in response to 2 μM CCh stimulation in HEK-293 cells in the presence or absence of 1μM A839977. Prestimulus $[Ca^{2+}]_i$ values for representative control and treated cell traces were 60.83 nM (CCh) and 63.75 nM (CCH + A839977) respectively. **B.** Bar graph of rate of exocytosis in isolated parotid acinar cells upon 0.1, 2 and 10 μM CCh application with or without A839977 treatment. The number of secretory events was comparable across all groups. **C - E.** Line traces show $[Ca^{2+}]_i$ responses upon 0.1, 2 and 10 μM CCh application with or without A839977 treatment respectively. Prestimulus $[Ca^{2+}]_i$ values for control and treated cell traces were 98.5 nM (0.1 μM CCh) and 94.8 nM (0.1 μM CCh + A839977), 107.1 nM (2 μM CCh) and 147.7 nM (2 μM CCh + A839977) and 142.7 nM (10 μM CCh) and 285.1 nM (10 μM CCh + A839977) respectively. **F.** Bar diagram shows maximal Δ $[Ca^{2+}]_i$ upon CCh application with or without A989977 treatment during 0.1, 2 and 10 μM CCh treatment. $[Ca^{2+}]_i$ responses were significantly decreased in groups treated with 2 μM ($p < 0.009$) or 10 μM ($p < 0.05$) CCh in the presence of A839977 when compared to those treated with CCh alone. Prestimulus $[Ca^{2+}]_i$ values for control and treated bars were 121.3 ± 2.7 nM (0.1 μM CCh) and 84.5 ± 9.6 nM (0.1 μM CCh + A839977), 176.7 ± 20.5 nM (2 μM CCh) and 209.1 ± 47 nM (2 μM

CCh + A839977) and 142.4 ± 14.2 nM (10 μM CCh) and 202.4 ± 41.7 nM (10 μM CCh + A839977) respectively. These data show a diminishment in CCh evoked $[Ca^{2+}]_i$ signals upon P2X7R inhibition in parotid acini.